POLİTEKNİK DERGİSİ

JOURNAL of POLYTECHNIC

ISSN: 1302-0900 (PRINT), ISSN: 2147-9429 (ONLINE)
URL: http://dergipark.org.tr/politeknik

The effect of turbulence model and nanofluid on fluid flow and heat transfer in a narrow rectangular duct

Dar dikdörtgensel bir kanalda türbülans modelinin ve nanoakışkanın ısı transferine ve akışkan akışına etkisinin sayısal olarak incelenmesi

***Yazar(lar) (Author(s))**: Edaviye Sare AKBAY[1], Berkay DERELI[2], Oguz TURGUT[3]*

ORCID[1]: 0000-0003-0000-8662

ORCID[2]: 0000-0001-6888-5923

ORCID[3]: 0000-0001-5480-1039

Bu makaleye şu şekilde atıfta bulunabilirsiniz(To cite to this article): Akbay E. S., Dereli B. and Turgut O., "The effect of turbulence model and nanofluid on fluid flow and heat transfer in a narrow rectangular duct", ***Politeknik Dergisi***, 23(2): 567-579, (2020).

Erişim linki (To link to this article): http://dergipark.org.tr/politeknik/archive

DOI: **10.2339/politeknik.589390**

The Effect of Turbulence Model and Nanofluid on Fluid Flow and Heat Transfer in a Narrow Rectangular Duct

Araştırma Makalesi / Research Article

Edaviye Sare AKBAY, Berkay DERELI, Oguz TURGUT*

Gazi University, Faculty of Engineering, Department of Mechanical Engineering & Clean Energy Research and Application Center (TEMENAR), Maltepe, Ankara, Turkey

(Geliş/Received : 09.07.2019 ; Kabul/Accepted : 06.09.2019)

ABSTRACT

The effect of type of turbulence model and nanofluid on the heat transfer and fluid flow in a horizontal narrow rectangular duct is numerically studied under constant wall heat flux boundary condition. Numerical study is carried out using ANSYS Fluent 17.0 software. Examined parameters are the type of turbulence model, the type of nanofluid, the volume fraction of nanoparticle in nanofluid, and the Reynolds number. Three different k-ε and four different k-ω turbulence models are employed. Aluminum oxide Al_2O_3-water and copper oxide CuO-water are used as nanofluids. Volume fractions of nanoparticles used are 0%, 0.1%, 0.5%, 1%, 2% and 4%. Reynolds number changes from 3×10^3 to 50×10^3. Results showed that k-ω standard turbulence model with low Reynolds number correction gives better result. It is seen that both the type and the volume fraction of nanoparticle in nanofluid affect heat transfer and pressure drop. Using Al_2O_3 and CuO nanoparticles in water increases thermal performance. It is found that the performance factor of CuO-water nanofluid is better than that of Al_2O_3-water nanofluid. It is seen that using turbulent fully developed flow correlations derived for circular ducts may end up with incorrect results for the flow in two-dimensional rectangular duct.

Keywords: Computational fluid dynamics (CFD), turbulent flow, nanofluid, heat source, numerical analysis.

Dar Dikdörtgensel Bir Kanalda Türbülans Modelinin ve Nanoakışkanın Isı Transferine ve Akışkan Akışına Etkisinin Sayısal Olarak İncelenmesi

ÖZ

Türbülans modelinin ve nanoakışkanın, yatay dar dikdörtgen bir kanaldaki ısı transferi ve akışkan akışı üzerindeki etkisi duvarda sabit ısı akısı sınır koşulu altında sayısal olarak incelenmiştir. Sayısal çalışma ANSYS Fluent 17.0 yazılımı kullanılarak gerçekleştirilmiştir. İncelenen parametreler türbülans modeli tipi, nanoakışkan tipi, nanoakışkanın hacim fraksiyonu ve Reynolds sayısıdır. Üç farklı k-ε ve dört farklı k-ω türbülans modeli kullanılmıştır. Nanoakışkan olarak alüminyum oksit Al_2O_3-su ve bakır oksit CuO-su kullanılmıştır. Kullanılan nanopartiküllerin hacim fraksiyonları %0, %0,1, %0,5, %1, %2 ve %4'tür. Reynolds sayısı 3×10^3'den 50×10^3'e değişmektedir. Sonuçlar, düşük Reynolds düzeltmeli k-ω standart türbülans modelinin daha iyi sonuç verdiğini göstermiştir. Nanoakışkanın hem tipinin hem de hacim fraksiyonunun ısı transferini ve basınç düşüşünü etkilediği görülmüştür. Su içerisinde Al_2O_3 ve CuO nanoparçacıklarının kullanılması ısıl performansı artırmıştır. CuO-su nanoakışkan performans faktörünün Al_2O_3-su nanoakışkanınkinden daha iyi olduğu görülmüştür. Dairesel kesitli kanallar için türetilen türbülanslı tam gelişmiş akış korelasyonlarının iki boyutlu dikdörtgen kanallar için kullanılmasının yanlış sonuçlar verebileceği görülmüştür.

Anahtar Kelimeler: Hesaplamalı akışkanlar dinamiği (HAD), türbülanslı akış, nanoakışkan, ısı kaynağı, sayısal analiz.

1. INTRODUCTION

The correlations obtained for turbulent flow in a circular duct are used for noncircular ducts using hydraulic diameter. However, cross-sectional shape of a duct affects the flow and heat transfer characteristics. Therefore, using these correlations may give up to 35% higher values than real duct results [1,2]. Also, the type of fluid affects flow and heat transfer characteristics. In order to increase heat transfer rate, nanoparticles such as Al_2O_3, CuO, TiO_2 etc. are used in base fluids like ethylene glycol, oil, water etc.

Forced convection heat transfer and fluid flow in two-dimensional rectangular ducts draw attention owing to its wide applications in many industrial systems such as nuclear reactors, heat exchangers, and electronic cooling systems.

Fully developed turbulent flow with two-dimensional heat transfer through solar air heater with protrusion wires was analyzed by Prasad and Saini [3]. Average Stanton number and average friction factor expressions

*Sorumlu Yazar (Corresponding Author)
e-posta : oturgut2006@gmail.com

were given. Yuan et al. [4] examined fully developed laminar air flow between two parallel plates with circular ribs at the upper and lower walls with a constant temperature. It was stated that using ribs on the walls increases both Nusselt number and pressure drop. Valencia et al. [5] studied unsteady laminar air flow in a two-dimensional duct with square ribs at constant temperature boundary condition. It was observed that ribs significantly affect the flow and heat transfer characteristics. Chaube et al. [6] numerically and experimentally investigated turbulent air flow using different viscous models in a two-dimensional rectangular duct having ribs on the bottom surface under constant heat flux thermal boundary condition. It was found that ribs significantly enhance heat transfer. Three-dimensional turbulent water flow in a ribbed duct was numerically investigated by Bayraktar et al. [7] using Reynolds stress turbulence model. Authors stated that ribs used on the surface of duct affect friction coefficient. Sohankar [8] numerically investigated two-dimensional turbulent flow and heat transfer in a channel with ribs in staggered arrangement. Results show that heat transfer is significantly affected by turbulent Prandtl number. Ahmed et al. [9] investigated two-dimensional laminar flow of nanofluids using ethylene glycol as base fluid in a triangular duct with vortex generator. It was found that nanofluid increases Nusselt number. Yadav and Bhagoria [10] numericaly analyzed two-dimensional turbulent flow and heat transfer along solar air heater with circular ribs. It was stated that relative roughness pitch increases thermohydraulic performance parameter. Yadav and Bhagoria [11] numerically studied two-dimensional CFD analysis of turbulent flow along a solar air heaters that have different shapes of square-sectioned ribs on the absorber plate. It was stated that relative roughness height affects flow friction, heat transfer and thermohydraulic performance parameter. Jhariya et al. [12] numerically investigated two-dimensional turbulent flow and heat transfer in a solar air heater with semi-circular ribs placed on the upper wall. Authors found that heat transfer increases with increasing relative roughness pitch. Albojamal et al. [13] numerically investigated two-dimensional laminar flow in a wavy duct using Al_2O_3-water and CuO-water nanofluids. It was found that particle volume fraction in nanofluid increases heat transfer. Turgut and Arslan [14] studied laminar air flow in a two-dimensional duct with staggered fins. Authors concluded that using fins on the surfaces of duct is not advantageous for two-dimensional periodically fully developed laminar flow. Mahanand et al. [15] conducted a numerical study to survey two-dimensional heat transfer along solar air heater with semi-circular ribs. It was found that roughness increases heat transfer and friction factor. Sahu et al. [16] investigated turbulent air flow in the two-dimensional duct with triangular protrusions located in the heated lower wall. It was concluded that using triangular protrusions causes higher heat transfer and pressure drop.

It is seen that there is a lack of information about which turbulence model gives the best results, how the type of nanofluid affects the turbulent flow and heat transfer characteristics in a narrow rectangular duct, and whether the correlations obtained for a circular cross-sectional duct can be used for fluid flow in a narrow rectangular duct. Therefore, the effect of turbulence model and the type of nanofluid on fluid flow and heat transfer characteristics in a two-dimensional duct are investigated numerically under constant heat flux boundary condition. Four different k-ω turbulence models (k-ω standart and k-ω SST turbulence models with and without low Reynolds number correction) and three different k-ε turbulence models (k-ε RNG, k-ε standart, k-ε realizable) are used. Heat transfer and fluid flow are examined using two different nanofluids (Al_2O_3-water and CuO-water). The novelty of this study is the comparison of the results of different turbulence models and determining the appropriate turbulence model for the flow in a narrow rectangular duct. Another novelty of this study is the comparison of the performance parameters of Al_2O_3-water and CuO-water nanofluids. In addition, whether the correlations obtained for a circular duct can be used for fluid flow in a narrow rectangular duct using hydraulic diameter is the another novelty of this study.

2. METHODS AND ANALYSIS

2.1. Governing Equations

In this study, two-dimensional turbulent flow in the rectangular duct is considered. Geometrical shape of two-dimensional smooth duct is shown in Figure 1. Coordinate axis used in this study is also shown in Figure 1. Fluid flows in the x-direction. The duct is divided into two sections i.e. entry section and test section. In Figure 1, H is the duct height and taken as 0.020 m. L1 and L2 are the lengths of the entry and test sections, respectively. The lengths of the entry section L1 and test section L2 are choosen more than ten times of hydraulic diameter to provide hydrodynamically and thermally fully developed flow conditions. Entry section is used to obtain hydrodynamically fully developed conditions at the inlet of the test section. Constant heat flux boundary condition is applied to the walls of the test section. Hydraulic diameter D_h is taken as D_h=2H. L1/D_h and L2/D_h are taken as 25 and 37.5, respectively.

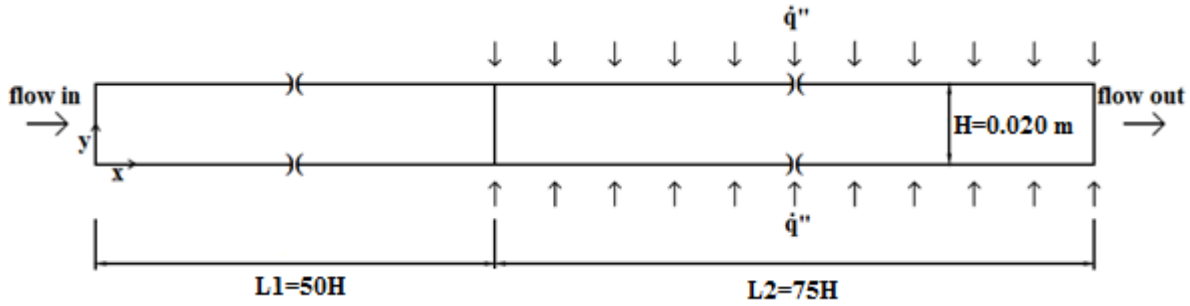

Figure 1. Schematic of two-dimensional smooth duct

Two-dimensional numerical analysis is performed assuming steady state, incompressible, Newtonian fluid with negligible viscous dissipation, and buoyancy effects. Governing equations are the continuity, momentum, energy, and turbulence model equations. These equations are given as below;

Continuity equation;

$$\frac{\partial}{\partial x_i}(\rho u_i) = 0 \tag{1}$$

Momentum equation;

$$\frac{\partial}{\partial x_j}(\rho u_i u_j) = -\frac{\partial p}{\partial x_i} + \frac{\partial}{\partial x_j}\left[\mu\left(\frac{\partial u_i}{\partial x_j} + \frac{\partial u_j}{\partial x_i}\right)\right] + \frac{\partial}{\partial x_j}\left(-\rho\overline{u_i' u_j'}\right) \tag{2}$$

Energy equation;

$$\frac{\partial}{\partial x_j}(\rho u_j T) = \frac{\partial}{\partial x_j}\left(k_{eff}\frac{\partial T}{\partial x_j}\right) \tag{3}$$

where k_{eff} is the effective thermal conductivity. The equations given above are solved together with the equations of turbulence model. Average Reynolds stress $\left(-\rho\overline{u_i' u_j'}\right)$ in momentum equation and turbulent heat flux $\rho u_j T$ in energy equation are expressed by a suitable turbulence model. The Reynolds stress is expressed as follows

$$-\rho\overline{u_i' u_j'} = -\rho\frac{2}{3}k\delta_{ij} + \mu_t\left(\frac{\partial u_i}{\partial x_j} + \frac{\partial u_j}{\partial x_i}\right) \tag{4}$$

2.2. Turbulence Models

Turbulence models used are the three types of k-ε turbulence models (standard, RNG and realizable) and four types of k-ω turbulence models (standard and SST with and without low Reynolds number correction) in ANSYS Fluent 17.0 [17].

Standard k-ε turbulence model

Transport equations for standard k-ε turbulence model proposed by Launder and Spalding [18] are given as

$$\frac{\partial}{\partial x_i}(\rho k u_i) = \frac{\partial}{\partial x_j}\left[\left(\mu + \frac{\mu_t}{\sigma_k}\right)\frac{\partial k}{\partial x_j}\right] - \rho\overline{u_i' u_j'}\frac{\partial u_j}{\partial x_i} - \rho\varepsilon \tag{5}$$

$$\frac{\partial}{\partial x_i}(\rho\varepsilon u_i) = \frac{\partial}{\partial x_j}\left[\left(\mu + \frac{\mu_t}{\sigma_\varepsilon}\right)\frac{\partial \varepsilon}{\partial x_j}\right] - C_{1\varepsilon}\frac{\varepsilon}{k}\rho\overline{u_i' u_j'}\frac{\partial u_j}{\partial x_i} - C_{2\varepsilon}\rho\frac{\varepsilon^2}{k} \tag{6}$$

Here, σ_ε and σ_k point out the turbulent Prandtl numbers for ε and k, respectively. μ_t is the turbulent (eddy) viscosity and computed as

$$\mu_t = \rho C_\mu k^2/\varepsilon \tag{7}$$

Model constants are: $C_{1\varepsilon}$=1.44, $C_{2\varepsilon}$=1.92, C_μ=0.09, σ_ε=1.3 and σ_k=1.0.

RNG k-ε turbulence model

Transport equations for RNG k-ε turbulence model are as follows [19]

$$\frac{\partial}{\partial x_i}(\rho k u_i) = \frac{\partial}{\partial x_j}\left[\alpha_k\left(\mu + \frac{\mu_t}{\sigma_k}\right)\frac{\partial k}{\partial x_j}\right] - \rho\overline{u_i' u_j'}\frac{\partial u_j}{\partial x_i} - \rho\varepsilon \tag{8}$$

$$\frac{\partial}{\partial x_i}(\rho\varepsilon u_i) = \frac{\partial}{\partial x_j}\left[\alpha_\varepsilon\left(\mu + \frac{\mu_t}{\sigma_\varepsilon}\right)\frac{\partial \varepsilon}{\partial x_j}\right] - C_{1\varepsilon}\frac{\varepsilon}{k}\rho\overline{u_i' u_j'}\frac{\partial u_j}{\partial x_i} - C_{2\varepsilon}^*\rho\frac{\varepsilon^2}{k} \tag{9}$$

where $C_{2\varepsilon}^* = C_{2\varepsilon} + \frac{C_\mu\eta^3(1-\eta/4.38)}{1+0.012\eta^3}$ with $\eta = Sk/\varepsilon$, $S = \sqrt{2S_{ij}S_{ij}}$. μ_t is the turbulence viscosity and determined from Eq. (7) with C_μ=0.0845. Model constants are $C_{1\varepsilon}$=1.42, $C_{2\varepsilon}$=1.68, $\alpha_k = \alpha_\varepsilon$=1.393, σ_ε=1.3 and σ_k=1.0.

Realizable k-ε turbulence model

Transport equations for k and ε in realizable k-ε turbulence model are given as [20]

$$\frac{\partial}{\partial x_j}\left(\rho k u_j\right)=\frac{\partial}{\partial x_j}\left[\left(\mu+\frac{\mu_t}{\sigma_k}\right)\frac{\partial k}{\partial x_j}\right]-\rho\overline{u_i' u_j'}\frac{\partial u_j}{\partial x_i}-\rho\varepsilon \quad (10)$$

$$\frac{\partial}{\partial x_j}\left(\rho\varepsilon u_j\right)=\frac{\partial}{\partial x_j}\left[\left(\mu+\frac{\mu_t}{\sigma_\varepsilon}\right)\frac{\partial \varepsilon}{\partial x_j}\right] +\rho C_1 S\varepsilon-\rho C_2\varepsilon^2/\left(k+\sqrt{\nu\varepsilon}\right) \quad (11)$$

Here, $C_1=\max\left[0.43,\eta/(\eta+5)\right]$ with $\eta=Sk/\varepsilon$ and $S=\sqrt{2S_{ij}S_{ij}}$. μ_t is the eddy viscosity and computed from Eq. (7) with $C_\mu=1/\left(4.04+A_s kU^*/\varepsilon\right)$, $U^*=\sqrt{S_{ij}S_{ij}+\Omega_{ij}\Omega_{ij}}$, $A_s=\sqrt{6}\cos\varphi$, $\Omega_{ij}=\frac{1}{2}\left(\frac{\partial u_i}{\partial x_j}-\frac{\partial u_j}{\partial x_i}\right)$, $\varphi=\frac{1}{3}\cos^{-1}\left(\sqrt{6}W\right)$, $W=S_{ij}S_{jk}S_{ki}/\bar{S}^3$, $\bar{S}=\sqrt{2S_{ij}S_{ij}}$, $S_{ij}=\frac{1}{2}\left(\frac{\partial u_j}{\partial x_i}+\frac{\partial u_i}{\partial x_j}\right)$. The model constants are C_2=1.9, σ_k=1.0, σ_ε=1.2.

Standard k-ω model

ANSYS Fluent uses the Wilcox [21] k-ω model as standard k-ω model, and transport equations are given as

$$\frac{\partial}{\partial x_i}\left(\rho k u_i\right)=\frac{\partial}{\partial x_j}\left[\left(\mu+\frac{\mu_t}{\sigma_k}\right)\frac{\partial k}{\partial x_j}\right]-\rho\overline{u_i' u_j'}\frac{\partial u_j}{\partial x_i} -\rho\beta_i^* f_{\beta^*} k\omega \quad (12)$$

$$\frac{\partial}{\partial x_i}\left(\rho\omega u_i\right)=\frac{\partial}{\partial x_j}\left(\left(\mu+\frac{\mu_t}{\sigma_\omega}\right)\frac{\partial \omega}{\partial x_j}\right) -\alpha\frac{\omega}{k}\rho\overline{u_i' u_j'}\frac{\partial u_j}{\partial x_i}-\rho\beta f_\beta\omega^2 \quad (13)$$

where σ_k and σ_ω represent the turbulent Prandl numbers for k and ω, respectively. μ_t is the turbulent viscosity and computed from

$$\mu_t=\alpha^*\rho k/\omega \quad (14)$$

where $\alpha^*=\alpha_\infty^*\left(\frac{0.024+\mathrm{Re}_t/6}{1+\mathrm{Re}_t/6}\right)$, $\mathrm{Re}_t=\frac{\rho k}{\mu\omega}$ and β=0.072.

In Eq. (12), $\beta_i^*=\beta_\infty^*\left(\frac{4/15+(\mathrm{Re}_t/8)}{1+(\mathrm{Re}_t/8)}\right)$ and

$$f_{\beta^*}=\begin{cases}1 & \chi_k\le 0\\ \frac{1+680\chi_k^2}{1+400\chi_k^2} & \chi_k>0\end{cases} \text{ with } \chi_k=\frac{1}{\omega^3}\frac{\partial k}{\partial x_j}\frac{\partial \omega}{\partial x_j}.$$

In Eq. (13), $\alpha=\frac{\alpha_\infty}{\alpha^*}\left(\frac{0.024+\mathrm{Re}_t/2.95}{1+\mathrm{Re}_t/2.95}\right)$ and

$$f_\beta=(1+70\chi_\omega)/(1+80\chi_\omega) \text{ with } \chi_\omega=\left|\frac{\Omega_{ij}\Omega_{jk}S_{ki}}{\left(\beta_\infty^*\omega\right)^3}\right|,$$

$\Omega_{ij}=\frac{1}{2}\left(\frac{\partial u_i}{\partial x_j}-\frac{\partial u_j}{\partial x_i}\right)$, $S_{ki}=\frac{1}{2}\left(\frac{\partial u_i}{\partial x_k}+\frac{\partial u_k}{\partial x_i}\right)$. In the high Reynolds number form of standard k-ω model, $\alpha^*=\alpha_\infty^*=1$, $\alpha=\alpha_\infty=1$ and $\beta_i^*=\beta_\infty^*$. Model constants are σ_k=2.0, σ_ω=2.0, β_∞^*=0.09.

Shear-stress transport (SST) k-ω model

ANSYS Fluent uses the SST k-ω model developed by Menter [22]. The SST k-ω model is based on both the standard k-ω model and the standard k-ε model. Transport equations for SST k-ω model are given as

$$\frac{\partial}{\partial x_i}\left(\rho k u_i\right)=\frac{\partial}{\partial x_j}\left[\left(\mu+\frac{\mu_t}{\sigma_k}\right)\frac{\partial k}{\partial x_j}\right]-\rho\overline{u_i' u_j'}\frac{\partial u_j}{\partial x_i} -\rho\beta^* k\omega \quad (15)$$

$$\frac{\partial}{\partial x_j}\left(\rho\omega u_j\right)=\frac{\partial}{\partial x_j}\left[\left(\mu+\frac{\mu_t}{\sigma_\omega}\right)\frac{\partial \omega}{\partial x_j}\right]-\frac{\alpha}{\nu_t}\rho\overline{u_i' u_j'}\frac{\partial u_j}{\partial x_i} -\rho\beta\omega^2+D_\omega \quad (16)$$

where μ_t is the turbulent viscosity and is computed as

$$\mu_t=\frac{\rho k}{\omega}\frac{1}{\max\left[\alpha^*, SF_2/a_1\omega\right]} \quad (17)$$

where $\alpha^*=\alpha_\infty^*\left(\frac{0.024+\mathrm{Re}_t/6}{1+\mathrm{Re}_t/6}\right)$ with $\mathrm{Re}_t=\frac{\rho k}{\mu\omega}$, $S=\sqrt{2S_{ij}S_{ij}}$, $S_{ij}=\frac{1}{2}\left(\frac{\partial u_j}{\partial x_i}+\frac{\partial u_i}{\partial x_j}\right)$. In the high Reynolds number form of SST k-ω model $\alpha^*=\alpha_\infty^*=1$. In Eqs. (15) and (16), σ_k and σ_ω are the turbulent Prandtl numbers for k and ω, respectively, and computed from $\sigma_k=1/\left(F_1/\sigma_{k,1}+(1-F_1)/\sigma_{k,2}\right)$ and $\sigma_\omega=1/\left(F_1/\sigma_{\omega,1}+(1-F_1)/\sigma_{\omega,2}\right)$. The blending functions

F_1 and F_2 are given by $F_1=\tanh\left(\varphi_1^4\right)$ and $F_2=\tanh\left(\varphi_2^2\right)$ with $\varphi_1=\min\left[\max\left(\frac{\sqrt{k}}{0.09\omega y},\frac{500\mu}{\rho y^2\omega}\right),\frac{4\rho k}{\sigma_{\omega,2}D_\omega^+ y^2}\right]$, $D_\omega^+=\max\left[2\rho\frac{1}{\sigma_{\omega,2}}\frac{1}{\omega}\frac{\partial k}{\partial x_j}\frac{\partial\omega}{\partial x_j},10^{-10}\right]$, $\varphi_2=\max\left[2\frac{\sqrt{k}}{0.09\omega y},\frac{500\mu}{\rho y^2\omega}\right]$. y is the distance to the next surface. In Eq. (15), $\beta^*=\beta_i^*=0.09\left(\frac{4/15+(Re_t/8)^4}{1+(Re_t/8)^4}\right)$. In Eq. (16), $\alpha=\frac{\alpha_\infty}{\alpha^*}\left(\frac{1/9+Re_t/2.95}{1+Re_t/2.95}\right)$ with $\alpha_\infty=F_1\alpha_{\infty,1}+(1-F_1)\alpha_{\infty,2}$, $\alpha_{\infty,1}=\beta_{i,1}/\beta_\infty^*-\kappa^2/\sigma_{\omega,1}\sqrt{\beta_\infty^*}$, $\alpha_{\infty,2}=\beta_{i,2}/\beta_\infty^*-\kappa^2/\sigma_{\omega,2}\sqrt{\beta_\infty^*}$, $\kappa=0.41$. In the high Reynolds number form $\alpha=\alpha_\infty=1$. In Eq. (16), $\beta=\beta_i=F_1\beta_{i,1}+(1-F_1)\beta_{i,2}$ and $D_\omega=2(1-F_1)\rho\frac{1}{\omega\sigma_{\omega,2}}\frac{\partial k}{\partial x_j}\frac{\partial\omega}{\partial x_j}$. Model constants; $\sigma_{k,1}=1.176$, $\sigma_{\omega,1}=2.0$, $\sigma_{k,2}=1.0$, $\sigma_{\omega,2}=1.168$, $a_1=0.31$, $\beta_{i,1}=0.075$, $\beta_{i,2}=0.0878$.

2.3. Boundary Conditions

The governing equations given above are solved using suitable boundary conditions at the boundaries of the computational domain given in Figure 1. In order to save time and memory, entry section and test section are solved separately. Firstly, entry section is solved. At the inlet (x=0), fluid enters the entry section at a uniform velocity. No-slip bounday condition is applied to the walls of the entry section for velocity. The pressure outlet boundary condition of ANSYS Fluent 17.0 is used at the outlet of the entry section, at x=L1. The values of variables are recorded in a file. After entry section, the test section is solved. The values read from this file are given as input at the inlet, at x=L1, of the test section. Fluid at the inlet of the test section is assumed at a uniform and constant temperature, i.e. T_i=293.15K. No-slip boundary condition is assumed at the walls of the test section for velocity. Constant heat flux boundary condition, $\dot{q}$"=1000W/m^2, is applied to the walls of the test section. At the outlet of the test section, i.e. at x=L1+L2, pressure outlet boundary condition of ANSYS Fluent 17.0, i.e. zero gradient for all variables, is applied.

For inlet and outlet boundary conditions, turbulent kinetic energy k [23], turbulent dissipation rate ε [17] and specific dissipation rate ω [17] are computed, respectively, as

$$k = 0.005U_i^2 \quad (18)$$

$$\varepsilon = C_\mu^{0.75}k^{1.5}/0.07D_h \quad (19)$$

$$\omega = k^{0.5}/C_\mu^{0.25}0.07D_h \quad (20)$$

Here, C_μ=0.09.

2.4. Numerical Method

ANSYS Fluent 17.0 software is used for numerical analysis. Grid (mesh) independence study is conducted in order to reach the correct results. Average Nusselt number and average Darcy friction factor values are calculated for comparison at different mesh numbers. Mesh number is changed between 74,021 and 468,961. Grid optimization study is carried out for the highest Reynolds number, which is Re=5×10^4. Fine mesh is generated near the walls, at the inlet and at the outlet. Coarse mesh is used away from the walls, inlet section and outlet section. The value of y+ is about unity. Mesh is generated using ANSYS Meshing. Typical mesh distribution in computational domain is shown in Figure 2a. As seen in Figure 2a, quadrilateral cells are created in the computational domain, and a non-uniform grid distribution is used. Inflation layers are used near the walls to capture the near wall parameters. Four different meshes are generated from the coarse element size, 74,021, to the fine element size, 468,961. Typical calculated average Nusselt number and average Darcy friction factor values are given in Figure 2b as a function of mesh number for RNG k-ε turbulence model. It is seen that the values of Nusselt number and Darcy friction factor almost remain constant after a certain mesh number. That is, the mesh number after which Nusselt number and Darcy friction factor do not change significantly is taken as optimum mesh number. According to Figure 2b, second mesh whose mesh number is 137,784 is chosen as optimum mesh. Calculations are conducted for other Reynolds numbers using this optimum mesh.

Second order upwing scheme is used for discretization of continuity, momentum, energy, and turbulence equations. SIMPLE algorithm is selected for pressure-velocity coupling. Solution is lasted for the residuals of pressure, velocity, k-ε or k-ω turbulence terms, and energy until 1×10^{-6}.

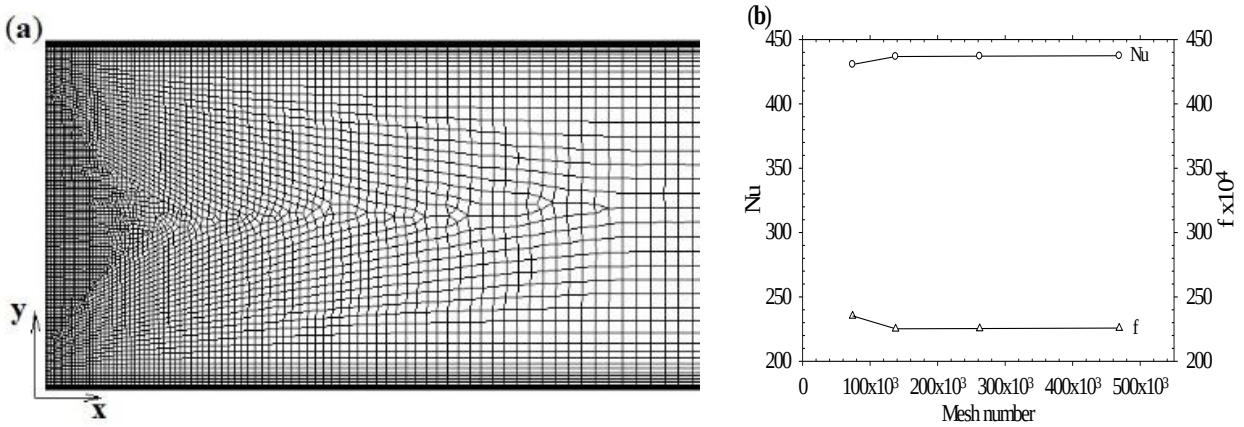

Figure 2. (a) Schematic view of mesh, (b) Nusselt number and Darcy friction factor versus mesh number

2.5. Calculated Parameters and Properties of Nanofluids

Reynolds number based on inlet velocity and hydraulic diameter is calculated as

$$Re = \rho U_i D_h / \mu \tag{21}$$

where ρ is the fluid density, U_i is the inlet velocity, D_h is the hydraulic diameter (D_h=2H), and μ is the dynamic viscosity of the fluid. Reynolds number varies from 3×10^3 to 5×10^4. Local Darcy friction factor and local Nusselt number are calculated, respectively, as

$$f_x = 8\tau_{w,x} \Big/ \rho U_i^2 \tag{22}$$

$$Nu_x = \dot{q}'' D_h \Big/ \left((T_w - T_b)_x K \right) \tag{23}$$

Average Darcy friction factor f and average Nusselt number Nu are computed, respectively, as

$$f = 2\Delta P D_h \Big/ L_2 \rho U_i^2 \tag{24}$$

$$Nu = \frac{\dot{q}'' D_h}{(T_w - T_b) K} = \frac{h D_h}{K} \tag{25}$$

Here ΔP is the pressure loss along the duct, L_2 is the test section length, $\dot{q}''$ is the wall heat flux, T_w and T_b are the wall and fluid bulk mean temperatures, respectively.

Water is used as base fluid while Al_2O_3 and CuO are used as nanoparticles. Density ρ [13, 24-28], dynamic viscosity μ [27], specific heat c_p [24, 28-29] and thermal conductivity K [25-26, 30] of nanofluids are calculated, respectively, as follows

$$\rho_{nf} = (1\text{-vof})\rho_{bf} + (\text{vof})\rho_p \tag{26}$$

$$\mu_{nf} = \mu_{bf} (1 + 2.5 \cdot \text{vof}) \tag{27}$$

$$c_{p,nf} = (1 - \text{vof}) \cdot c_{p,bf} + \text{vof} \cdot c_{p,p} \tag{28}$$

$$K_{nf} = K_{bf} \frac{K_p + 2K_{bf} - 2(K_{bf} - K_p) \cdot \text{vof}}{K_p + 2K_{bf} + 2(K_{bf} - K_p) \cdot \text{vof}} \tag{29}$$

In Eqs. (26-29), subscripts nf, bf and p indicate the nanofluid, base fluid and particle, respectively. vof is the volume fraction of nanoparticle in nanofluid. Physical properties of water are given in Table 1 at the temperature

Table 1. Physical properties of base fluid and nanoparticles

	ρ (kg/m^3)	μ (kg/m·s)	c_p (J/kg·K)	K (W/m·K)
Water	998	1002×10^{-6}	4182.0	0.598
Al_2O_3	3880	-	773	36
CuO	6500	-	535.6	20

293.15K [31-34].

3. RESULTS AND DISCUSSION

Typical local Nusselt number and local Darcy friction values are plotted in Figures 3a and b, respectively, at different Reynolds numbers for k-ε realizable turbulence model and vof=0%, i.e. for pure water. It is seen that local values of Nusselt number and Darcy friction factor begin with a high value, decrease along the duct, and approach to the constant value, i.e. fully developed value. Results indicate that Nusselt number increases with increasing Reynolds number while friction factor decreases.

Turbulent fully developed Nusselt number and Darcy friction factor correlations derived for fluid flow in a circular duct are given in Table 2 [31].

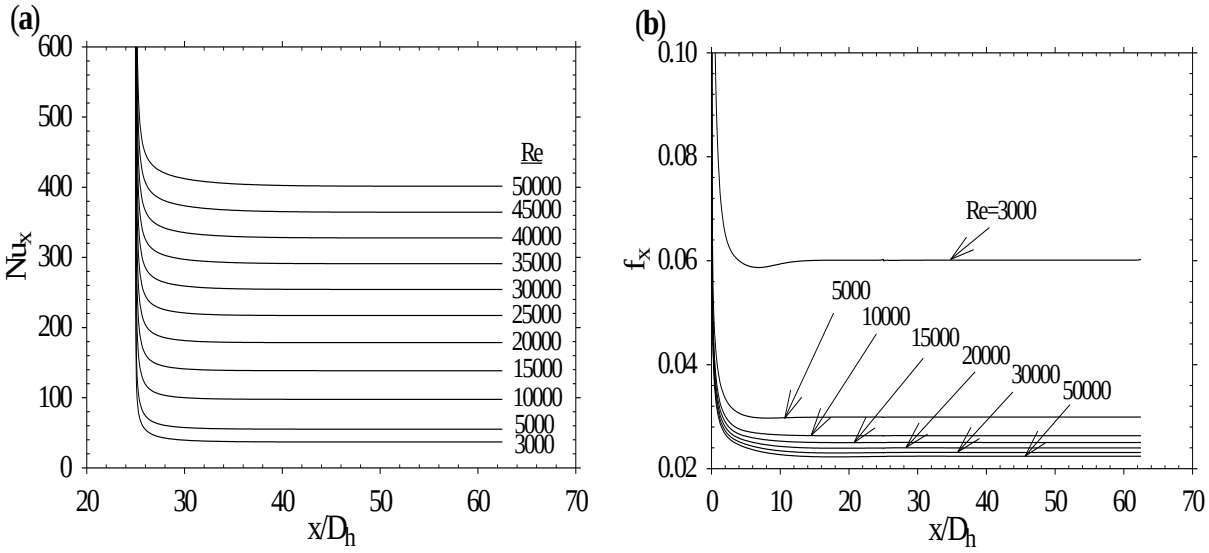

Figure 3. Local Nusselt number (a) and local Darcy friction factor (b) along the duct

Table 2. Fully developed correlations for Nu and f

$Nu_{fd}=\frac{(f/8)(Re-1000)Pr}{1+12.7(f/8)^{0.5}(Pr^{2/3}-1)}$	for $2300\le Re\le 5\times10^6$	Gnielinski	(30)
$Nu_{fd}=0.023Re^{0.8}Pr^{0.4}$	for $Re\ge 1\times10^4$	Dittus-Boelter	(31)
$Nu_{fd}=0.023Re^{0.8}Pr^{1/3}$	for $Re\ge 1\times10^4$	Colburn	(32)
$f_{fd}=0.316Re^{-0.25}$	for $Re\le 20\times10^3$	Moody	(33)
$f_{fd}=0.184Re^{-0.20}$	for $Re\ge 20\times10^3$	Moody	(34)
$f_{fd}=(0.790\ln Re-1.64)^{-2}$	for $3\times10^3\le Re\le 5\times10^6$	Petukhov	(35)

For all turbulence models studied, the fully developed Nusselt number and Darcy friction factor values are plotted in Figures 4a and b, respectively, as a function of Reynolds number for water at vof=0%. Fully developed Nusselt numbers and Darcy friction factors obtained from equations given in Table 2 are also shown in Figures 4a and b. Now, attention is firstly given to Figure 4a, which shows the fully developed Nusselt number values. It is seen that Nusselt number increases with increasing Reynolds number, as expected. Results show that the turbulence model which gives the closest value with the fully developed correlations given in Table 2 is the k-ω standard turbulence model with low Reynolds number correction. In addition, the fully developed correlation which gives the closest value with the values obtained from turbulence models is the Gnielinski equation, Eq. (30). At $Re=50\times10^3$, Gnielinski, Dittus-Boelter and Colburn equations give about 13, 24 and 33%, respectively, less values than the k-ω standard turbulence model with low Reynolds number correction. In other words, it is seen that using the correlations obtained for circular ducts may give incorrect results up to 33% for the flow in a two-dimensional rectangular duct. Similarly, k-ω standard with low Reynolds number correction, k-ω SST with low Reynolds number correction, k-ε realizable, k-ε standard, k-ω standard, k-ω SST, and k-ε RNG turbulence models give about 15, 21, 22, 24, 25, 27 and 57.8%, respectively, higher values than the Gnielinski equation, Eq. (30), at $Re=50\times10^3$. When the results of k-ω standard turbulence model with low Reynolds number correction and Gnielinski equation are compared, it is seen that the results are in harmony with each other.

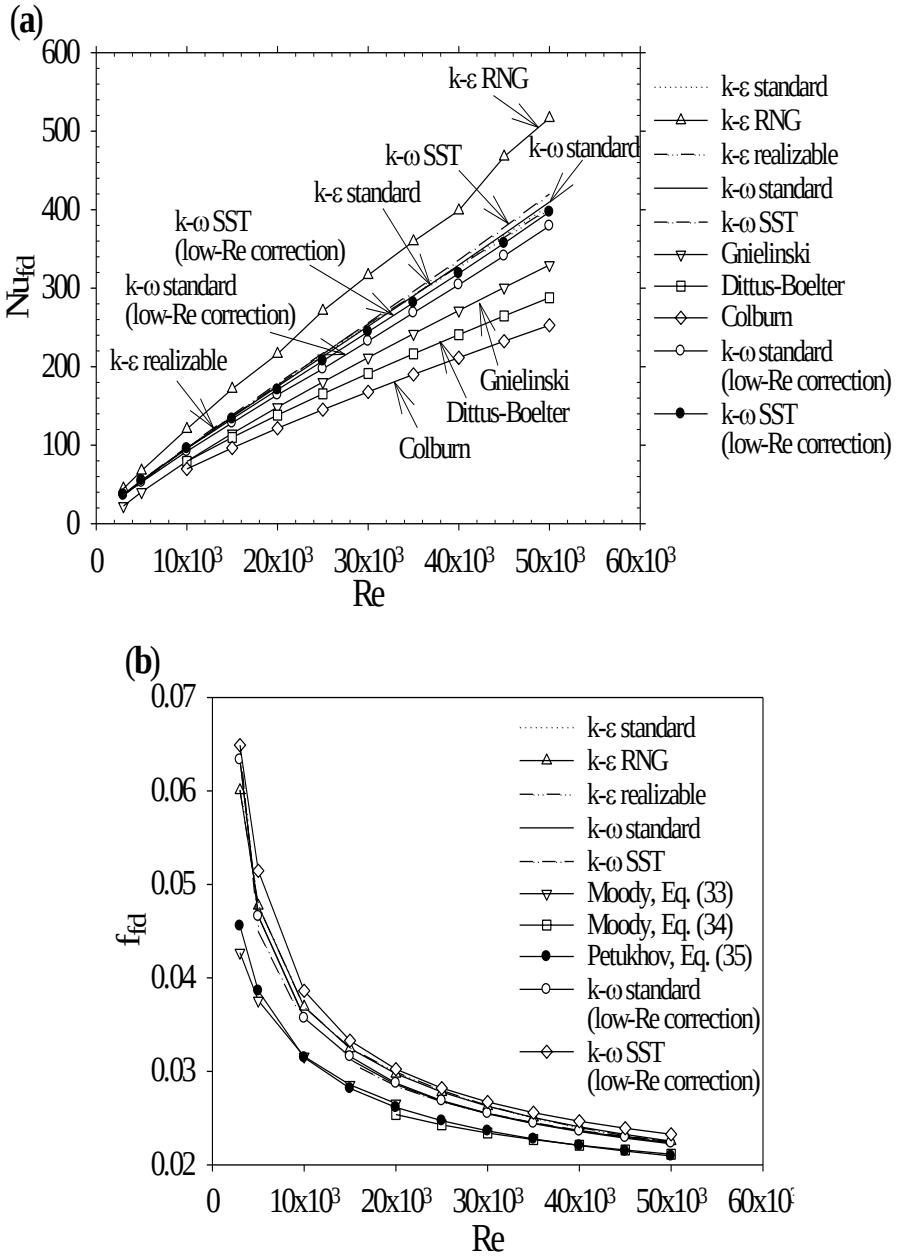

Figure 4. Fully developed Nusselt number (a) and Darcy friction factor (b) versus Reynolds number for different turbulence models

With regard to Figure 4b, which gives the fully developed Darcy friction factor values as a function of Reynolds number, results show that Darcy friction coefficient decreases with increasing Reynolds number, as expected. It is also seen that friction coefficient values for all cases are approximately the same. At $Re=50\times10^3$, Darcy friction factor value for k-ω standard turbulence model with low Reynolds number correction is about 6% higher than that of Moody, Eq. (34), and Petukhov, Eq. (35), equations. That is, Darcy friction factor for k-ω standard turbulence model with low Reynolds number correction agrees with the literature results.

After validation of the numerical study and choosing the best turbulence model, which is the k-ω standard turbulence model with low Reynolds number correction, Al_2O_3-water and CuO-water nanofluids in duct are investigated numerically using k-ω standard turbulence model with low Reynolds number correction. Results are given for the Reynolds number changing between 3×10^3 and 50×10^3 and volume fraction of nanoparticle ranging from 0 to 4%.

Figures 5a and b compare the variation of average heat transfer coefficient as a function of Reynolds number at different volume fractions of nanoparticles, vof, for Al_2O_3/water and CuO/water nanofluids, respectively. Results show that volume fraction of nanoparticles in nanofluid and Reynolds number affect heat transfer coefficient. It is seen that heat transfer coefficient

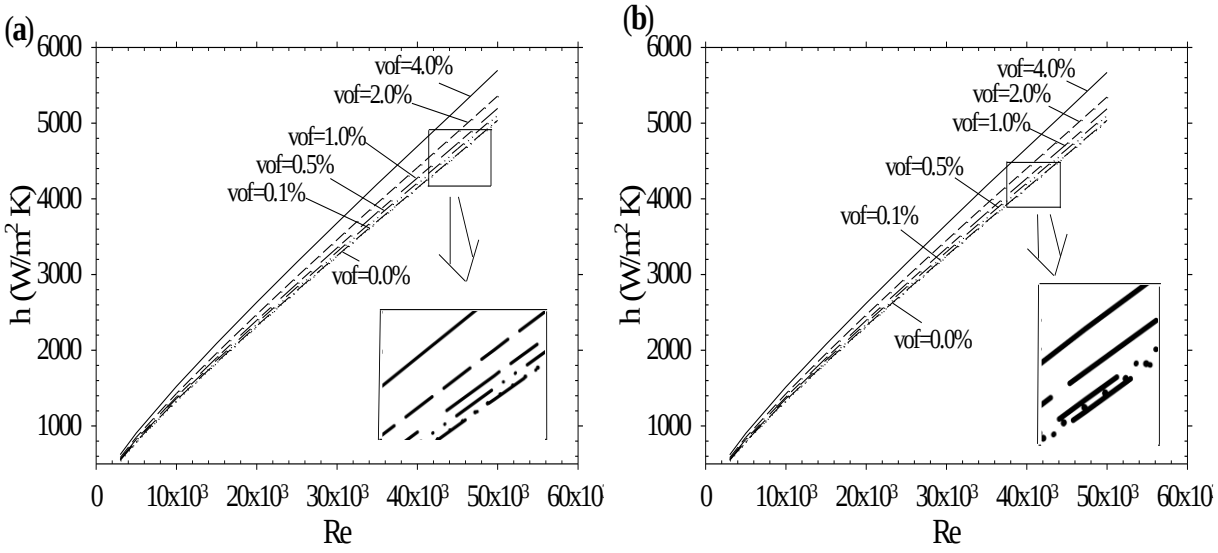

Figure 5. Average heat transfer coefficient versus Reynolds number for Al_2O_3/water nanofluid (a) and CuO/water nanofluid (b)

increases with increasing volume fraction of nanoparticle in nanofluid and Reynolds number for both nanofluids. That is, heat transfer coefficient increases with increasing Reynolds number at a given volume fraction of nanoparticle. It can be interpreted as that thermal boundary layer thickness decreases with increasing Reynolds number. Decreasing thermal boundary layer thickness results in increasing heat transfer. Also, heat transfer coefficient increases with increasing volume fraction of nanoparticle at a given Reynolds number. At $Re=50\times10^3$, heat transfer coefficient increases 13.1 and 12.6% for Al_2O_3-water and CuO-water nanofluids, respectively, when volume fraction of nanoparticle changes from 0 to 4%.

In order to see the effect of Reynolds number on convection heat transfer coefficient, average convection heat transfer coefficient is plotted in Figures 6a and b as a function of volume fraction of nanoparticle for Al_2O_3/water and CuO/water nanofluids, respectively. It is seen that two nanofluids show similar behavior. As seen in Figure 6, convection heat transfer coefficient increases with increasing nanoparticle in base fluid at a given Reynolds number for both nanofluids. It is also seen that convection heat transfer coefficient increases with increasing Reynolds number at a given volume fraction of nanoparticle in nanofluids. Figure 6a shows that heat transfer coefficient increases about 13.1% for Al_2O_3-water nanofluid when volume fraction of nanoparticle in nanofluid changes from 0 to 4% at Reynolds number $Re=50\times10^3$. With regard to Figure 6b, it is seen that changing of nanoparticle volume fraction of CuO-water nanofluid from 0 to 4% results in 12.6% enhancement in heat transfer coefficient at Reynolds number $Re=50\times10^3$. When the heat transfer coefficient

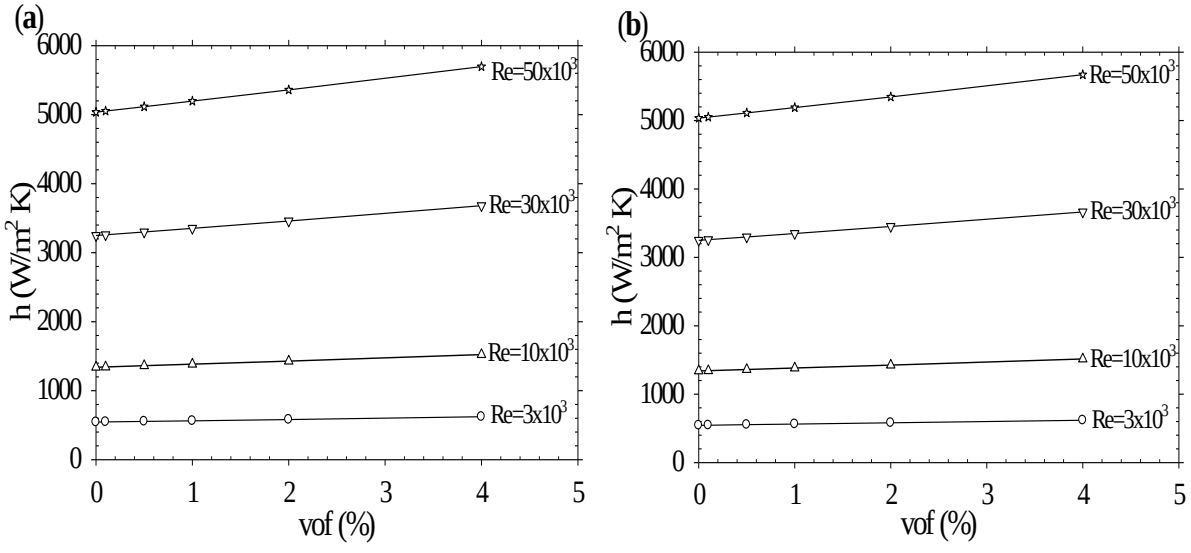

Figure 6. Average heat transfer coefficient versus vof for Al_2O_3/water nanofluid (a) and CuO/water nanofluid (b)

values of Al_2O_3-water nanofluid and CuO-water nanofluid are compared, it is seen that Al_2O_3-water nanofluid gives higher heat transfer coefficient than CuO-water nanofluid at a given Reynolds number and volume fraction of nanoparticle.

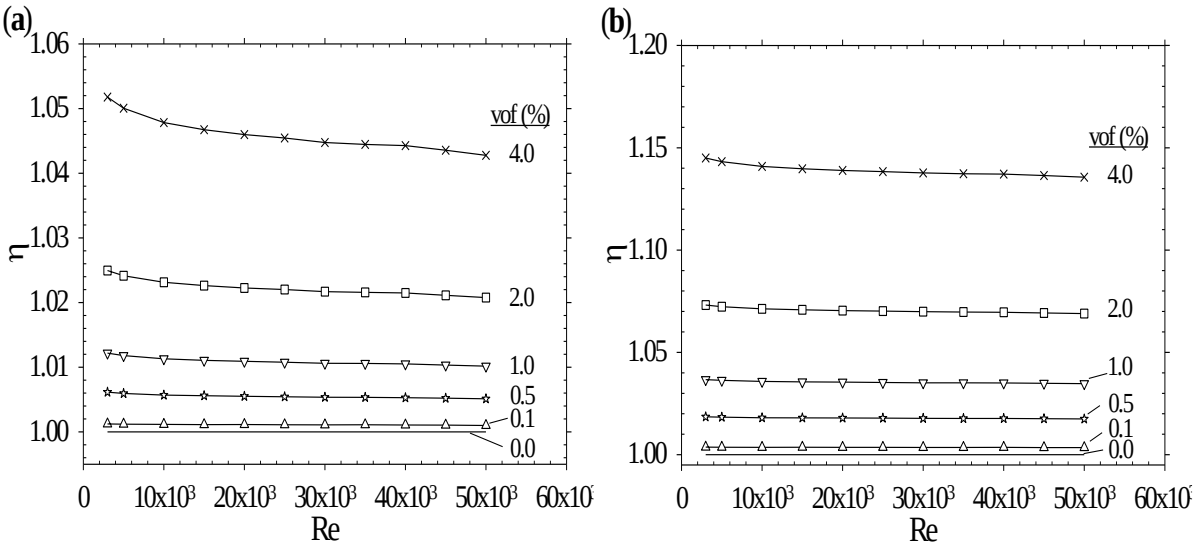

Figure 7. Performance factor for Al_2O_3/water nanofluid (a) and CuO/water nanofluid (b)

when the volume fraction of CuO/water nanofluid increases from 0 to 4% at a given Reynolds number. It is seen that pressure loss for Al_2O_3/water nanofluid is greater than that of CuO/water nanofluid.

Results show that both heat transfer coefficient and pressure loss increase when nanoparticle is added into base fluid. Increasing heat transfer is a desirable effect while increasing pressure loss in duct is an undesirable effect. Therefore, it is necessary to decide whether the use of Al_2O_3 and CuO nanoparticles in the water is appropriate or not. Performance factor, i.e. effective efficiency, gives the relationship between thermal and hydraulic characteristics of the nanofluid, and it is given as [35-37]

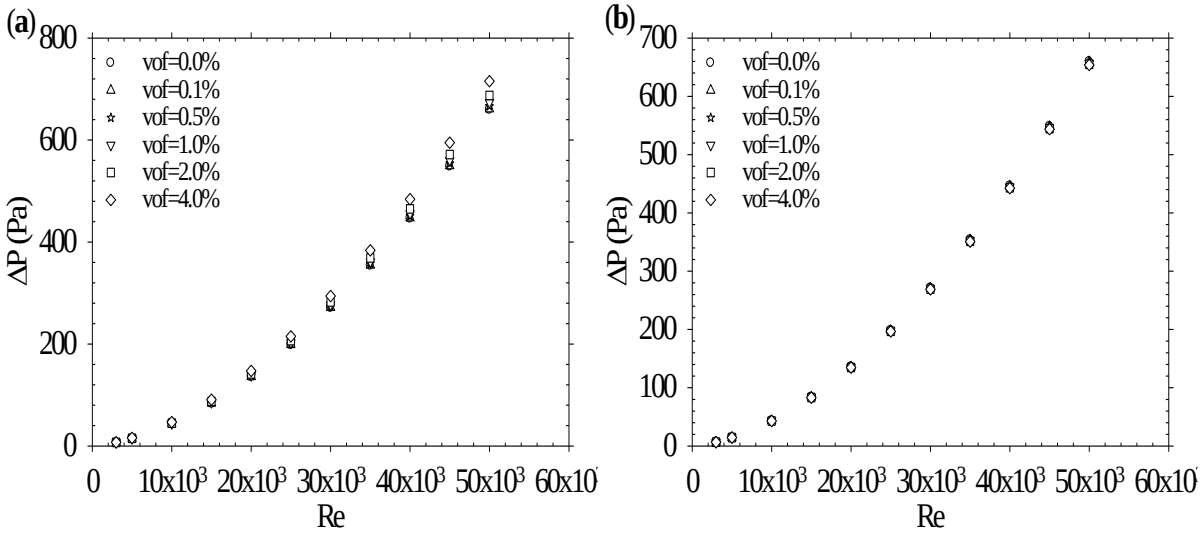

Figure 8. Pressure loss versus Re for Al_2O_3/water nanofluid (a) and CuO/water nanofluid (b)

To see the pressure loss along duct, pressure losses for Al_2O_3/water and CuO/water nanofluids are given in Figures 7a and b, respectively, as a function of Reynolds number at different volume fractions of nanoparticle. Figure 7 shows that pressure loss increases with increasing Reynolds number for both nanofluids. In addition, it is seen that pressure loss for Al_2O_3/water nanofluid increases with increasing volume fraction at the same Reynolds number. At $Re=50\times10^3$, pressure loss increases about 9% when volume fraction of Al_2O_3/water nanofluid increases from 0 to 4%. However, Figure 7b indicates that pressure loss does not change significantly

$$\eta = \left(h_{nf}/h_{bf}\right)/\left(\Delta P_{nf}/\Delta P_{bf}\right) \quad (36)$$

It is significant to calculate this value to see the effect of using nanoparticle in base fluid, water. The value of performance factor must be greater than 1.0 to apply nanoparticle addition to water. Thus, performance factor is calculated using Eq. (36) and plotted as a function of Reynolds number in Figures 8a and b for Al_2O_3/water and CuO/water nanofluids, respectively, at different nanoparticle volume fractions. It is seen that performance factor increases with increasing nanoparticle volume fraction for both nanofluids. It is also seen that performance factor decreases with increasing Reynolds number at a given nanoparticle fraction. As can be seen from Figures 8a and b, performance factor value is greater than unity. Thus, it can be said that the amount of heat transfer enhancement overcomes pressure loss, ie. pumping power. In other words, Al_2O_3 and CuO nanoparticle addition into water can be applied to increase heat transfer in a narrow rectangular duct. In addition, results show that CuO-water nanofluid has better thermal performance compared to Al_2O_3-water nanofluid.

4. CONCLUSION

Heat transfer and fluid flow characteristics of Al_2O_3-water and CuO-water nanofluids are numerically examined for turbulent flow in a two-dimensional rectangular duct. Numerical study is carried out using ANSYS Fluent 17.0 software. Three versions of k-ε and four versions of k-ω turbulence models of ANSYS Fluent 17.0 are used. Nanoparticle volume fraction in the range of 0-4.0% and Reynolds number changing from 3×10^3 to 50×10^3 are the examined parameters. Constant heat flux $\dot{q}"=1000$ W/m^2 boundary condition is applied to the walls of the duct. Results show that k-ω standard turbulence model with low Reynolds number correction gives the closest result compared to literature. It is seen that heat transfer increases with increasing both volume fraction of nanoparticles and Reynolds number. Pressure drop enhances with enhancing both nanoparticle volume fraction and Reynolds number as well. Results show that Al_2O_3-water nanofluid gives higher heat transfer coefficient than that of CuO-water nanofluid. In addition, Al_2O_3-water nanofluid has higher pressure loss in duct than that of CuO-water nanofluid. When the performance factor of Al_2O_3-water and CuO-water nanofluids are compared, it is seen that CuO-water nanofluid has better performance factor than that of Al_2O_3-water nanofluid. Thermal performance factor is greater than 1.0 for all Reynolds numbers and for all nanofluid fractions for two nanofluids. It can be said that Al_2O_3 and CuO nanoparticles can be added in water to increase the performance of water. It is seen that turbulent fully developed correlations derived for circular ducts may give incorrect results up to 33% for the flow in a two-dimensional rectangular duct.

NOMENCLATURE

D_h	Hydraulic diameter (m)
f	Average friction factor (-)
h	Average heat transfer coefficient (W/m^2·K)
H	Height of duct (m)
k	Turbulence kinetic energy (m^2/s^2)
k_{eff}	Effective thermal conductivity (W/m·K)
K	Thermal conductivity (W/m·K)
L	Length of duct (m)
Nu	Average Nusselt number (-)
P	Average pressure (Pa)
ΔP	Pressure drop along duct (Pa)
$\dot{q}"$	Heat flux (W/m^2)
Re	Reynolds number (-)
T	Temperature (K)
u_i	Average velocity in the i-direction (m/s)
u_j	Average velocity in the j-direction (m/s)
U_i	Inlet velocity (m/s)
u_i'	Fluctuating velocity component in i-direction (m/s)
u_j'	Fluctuating velocity component in j-direction (m/s)
vof	Volume concentration (-)
x_i	Coordinate system (m)

Greek Letters

δ_{ij}	Kronecker delta, -
ε	Turbulent dissipation rate (J/kg·s)
η	Thermohydraulic performance parameter (-)
μ	Dynamic viscosity (kg/m·s)
μ_t	Turbulent (eddy) viscosity (kg/m·s)
ρ	Density (kg/m^3)
σ_k	Turbulent Prandtl numbers for k (-)
σ_ε	Turbulent Prandtl numbers for ε (-)
τ	Shear stress on the wall (Pa)
ω	Specific dissipation rate (m^2/s^2)

Subscripts

b	Bulk
bf	Base fluid
fd	Fully developed
nf	Nanofluid
x	Local
w	Wall

REFERENCES

[1] Kakac S., Shah R.K. and Aung W., "Handbook of single-phase convective heat transfer", ***Wiley***, USA, (1987).

[2] He S. and Gotts J.A., "Calculation of friction coefficients for noncircular channels", ***ASME Journal of Fluids Engineering***, 126: 1033–1038, (2004).

[3] Prasad B.N. and Saini J.S., "Effect of artificial roughness on heat transfer and friction factor in a solar air heater", ***Solar Energy***, 41: 555-560, (1988).

[4] Yuan Z.X., Tao W.Q. and Wang Q.W., "Numerical prediction for laminar forced convection heat transfer in parallel-plate channels with streamwise-periodic rod disturbances", ***International Journal for Numerical Methods in Fluids***, 28: 1371-1387, (1998).

[5] Valencia A., Martin J.S. and Gormaz R., "Numerical study of the unsteady flow and heat transfer in channels

with periodically mounted square bars", ***Heat and Mass Transfer***, 37: 265-270, (2001).

[6] Chaube A., Sahoo P.K. and Solanki S.C., "Analysis of heat transfer augmentation and flow characteristics due to rib roughness over absorber plate of a solar air heater", ***Renewable Energy***, 31: 317–331, (2006).

[7] Bayraktar S., Bayraktar M. and Vardar N., "Numerical investigation of a water flow in a rib-roughened channel by using Reynolds stress model", ***International Journal of Computational Fluid Dynamics***, 22 (5): 331-339, (2008).

[8] Sohankar A., "Heat transfer and fluid flow through a ribbed passage in staggered arrangement", ***Iranian Journal of Science and Technology Transactions of Mechanical Engineering***, 34 (5): 471-485, (2010).

[9] Ahmed H.E., Mohammed H.A. and Yusoff M.Z., "Heat transfer enhancement of laminar nanofluids flow in a triangular duct using vortex generator", ***Superlattices and Microstructures***, 52: 398-415, (2012).

[10] Yadav A.S. and Bhagoria J.L., "A CFD based heat transfer and fluid flow analysis of a solar air heater provided with circular transverse wire rib roughness on the absorber plate", ***Energy***, 55: 1127–1142, (2013).

[11] Yadav A.S. and Bhagoria J.L., "Modeling and simulation of turbulent flows through a solar air heater having square-sectioned transverse rib roughness on the absorber plate", ***The Scientific World Journal***, ID 827131, (2013).

[12] Jhariya K., Ranjan R. and Paswan M.K., "A CFD based performance analysis of heat transfer enhancement in solar air heater provided with transverse semi-circular ribs", ***International Journal of Innovative Research in Science, Engineering and Technology,*** 4: 4528-4537, (2015).

[13] Albojamal A., Hamzah H., Haghighi A. and Vafai K., "Analysis of nanofluid transport through a wavy channel", ***Numerical Heat Transfer, Part A: Applications***, 72: 869-890, (2017).

[14] Turgut O. and Arslan K., "Periodically fully developed laminar flow and heat transfer in a 2-D horizontal channel with staggered fins", ***Thermal Science,*** 21: 2443-2455, (2017).

[15] Mahanand Y., Abhijit M. and Khamari D.S., "CFD analysis of semi-circular rib roughened solar air heater", ***International Journal of Advanced Mechanical Engineering***, 8: 251-262, (2018).

[16] Sahu M.K., Pandey K.M. and Chatterjee S., "Numerical investigation of thermal-hydraulic performance of channel with protrusions by turbulent cross flow jet", ***AIP Conference Proceedings***, 1966:020021, (2018).

[17] "ANSYS Fluent 17.0 Theory Guide", ***ANSYS Inc***, (2016).

[18] Launder B.E. and Spalding D.B., "Lectures in mathematical models of turbulence", ***Academic Press***, London, England, (1972).

[19] Yakhot V. and Orszag S.A., "Renormalization group analysis of turbulence I basic theory", ***Journal of Scientific Computing,*** 1: 1-51, (1986).

[20] Shih T.H., Liou W.W., Shabbir A., Yang Z. and Zhu J., "A new k-ε eddy-viscosity model for high Reynolds number turbulent flows", ***Computers Fluids***, 24: 227-238, (1995).

[21] Wilcox D.C., "Turbulence modeling for CFD", ***DCW Industries***, Inc. La Canada, California, (1998).

[22] Menter F.R., "Two-equation eddy-viscosity turbulence models for engineering applications", ***AIAA Journal***, 32: 1598-1605, (1994).

[23] Rokni M., "Numerical investigation of turbulent fluid flow and heat transfer in complex ducts", ***Doctoral thesis***, Lund University, Lund Institute of Technology, (1998).

[24] Pak B.C. and Cho Y.I., "Hydrodynamic and heat transfer study of dispersed fluids with submicron metallic oxide particles", ***Experimental Heat Transfer***, 11: 151-170, (1998).

[25] Ababaei A., Arani A.A.A. and Aghaei A., "Numerical investigation of forced convection of nanofluid flow in microchannels: effect of adding micromixer", ***Journal of Applied Fluid Mechanics***, 10: 1759-1772, (2017).

[26] Pourfattah F., Motamedian M., Sheikhzadeh G., Toghraie D. and Akbari O.A., "The numerical investigation of angle of attack of inclined rectangular rib on the turbulent heat transfer of water-Al2O3 nanofluid in a tube", ***International Journal of Mechanical Sciences***, 131-132: 1106-1116, (2017).

[27] Amanuel T. and Manish M., "Investigation of thermohydraulic performance of triple concentric-tube heat exchanger with CuO/water nanofluid: Numerical approach", ***Heat Transfer Asian Research***, 97: 974-995, (2018).

[28] Moraveji M.K., Barzegarian R., Bahiraei M., Barzegarian M., Aloueyan A. and Wongwises S., "Numerical evaluation on thermal–hydraulic characteristics of dilute heat-dissipating nanofluids flow in microchannels", ***Journal of Thermal Analysis and Calorimetry***, 135: 671–683, (2019).

[29] Moldoveanu G.M. and Minea A.A., "Specific heat experimental tests of simple and hybrid oxide-waternanofluids: proposing new correlation", ***Journal of Molecular Liquids***, 279: 299-305, (2019).

[30] Hamilton R.L. and Crosser O.K., "Thermal conductivity of heterogeneous two component systems", ***Industrial & Engineering Chemical Fundamentals***, 1: 187–191, (1962).

[31] Cengel Y.A. and Ghajar A.J., "Heat and mass transfer; fundamentals and applications", 4th edn., ***McGraw Hill***, New York, (2011).

[32] Praveen A., Babu P.S. and Mamilla V.R., "Analysis on heat transfer in nanofluids for Al_2O_3/water", ***International Journal of Advanced Scientific Research and Technology***, 2: 134-140, (2012).

[33] Arzani H.K., Arzani H.K., Kazi S.N. and Badarudin A., "Numerical study of developing laminar forced convection flow of water/CuO nanofluid in a circular tube with a 180 degree curve", ***World Academy of Science, Engineering and Technology, International Journal of Materials and Metallurgical Engineering***, 10: 795-802, (2016).

[34] Kezzar M., Nafir N., Tabel I. and Khanetout A., "A new analytical investigation of natural convection of non-Newtonian nanofluids flow between two vertical flat plates by the generalized decomposition method (GDM)", ***Journal of Thermal Engineering***, 4: 2490-2508, (2018).

[35] Pakdaman M.F., Akhavan-Behabadi M.A. and Razi P., "An experimental investigation on thermo-physical properties and overall performance of MWCNT/heat transfer oil nanofluid flow inside vertical helically coiled tubes", ***Experimental Thermal and Fluid Science***, 40: 103–111, (2012).

[36] Ahmed H.E., Yusoff M.Z., Hawlader M.N.A., Ahmed M.I., Salman B.H. and Kerbeetf A.Sh., "Turbulent heat transfer and nanofluid flow in a triangular duct with vortex generators", ***International Journal of Heat and Mass Transfer***, 105: 495-504, (2017).

[37] Boukerma K. and Kadja M., "Convective heat transfer of Al2O3 and CuO nanofluids using various mixtures of water-ethylene glycol as base fluids", ***Engineering, Technology & Applied Science Research***, 7: 1496-1503, (2017).